Applied Surface Science 487 (2019) 848–856

Contents lists available at ScienceDirect

Applied Surface Science

journal homepage: www.elsevier.com/locate/apsusc

Full length article

New aspects of the surface chemistry of sulfur on Au(111): Surface structures formed by gold-sulfur complexes

Pilar Carro[a], Gustavo Andreasen[b], Carolina Vericat[b], María Elena Vela[b], Roberto Carlos Salvarezza[b,*]

[a] Área de Química Física, Departamento de Química, Facultad de Ciencias, Universidad de La Laguna, Instituto de Materiales y Nanotecnología, Avda. Francisco Sánchez, s/n 38200-La Laguna, Tenerife, Spain

[b] Instituto de Investigaciones Fisicoquímicas Teóricas y Aplicadas (INIFTA), Facultad de Ciencias Exactas, Universidad Nacional de La Plata, CONICET, La Plata 1900, Argentina

ARTICLE INFO

Keywords:
Gold
Sulfur adsorption
Surface structures
Gold-sulfur complexes

ABSTRACT

Sulfur adsorption on gold surfaces has been extensively studied because of the key role of sulfur species in heterogeneous catalysis, and, more recently, due to the interest in the synthesis of anisotropic gold nanoparticles with potential applications in medicine that involves sulfide reduction. Here we report new surface structures for sulfur on Au(111) by combining in situ scanning tunneling microscopy in aqueous sodium sulfide solutions and density functional theory calculations. Our results show two related lattices, $(3\sqrt{3} \times 3\sqrt{3})$ R30° ($\theta = 0.22$) and $(\sqrt{7} \times \sqrt{7})$ R19.1° ($\theta = 0.57$), that involve AuS_3 complexes as building blocks. Gold-sulfur complexes are formed by the lifting of gold atoms from the substrate surface as revealed by density functional theory calculations. These species, intermediate between adsorbed S in the well-known $(\sqrt{3} \times \sqrt{3})$-R30° lattice and adsorbed polysulfides in organized rectangular structures, explain the surface coverage of gold vacancy islands, a fingerprint of S adsorption on Au(111).

1. Introduction

The adsorption of sulfur on gold surfaces has been extensively studied in the past years, in particular concerning the complex sulfur-gold surface chemistry and the different related surface structures [1–7]. This is especially relevant for different applications which range from heterogeneous catalysis, where S on gold nanoparticles can act either as a poison or as a catalyst depending on the reaction [1,8–11], to nanomedicine, where S species are the capping agent of gold triangular nanoprisms prepared by gold salt reduction with sulfide [12] and which are promising for photothermal therapies due to their strong absorption in the near-infrared region [13,14]. Also, S is very important for the stability of nanostructures, as mobile metal-S complexes enhance the coarsening on coinage metal surfaces [15].

It is now widely accepted that, as the surface coverage (θ) increases on the Au(111) surface, monomeric (atomic) sulfur species evolve from short rows ($\theta < 0.1$) [5] to (5×5) ($\theta = 0.28$) [6,16] and $(\sqrt{3} \times \sqrt{3})$ R30° ($\theta = 0.33$) lattices [17,18]. At higher coverage, polysulfide species are formed on the substrate which organize into quasi-rectangular structures ($\theta = 0.66$) [19] that coexist with a large number of Au vacancy islands, whose coverage θ_{vac} changes from ≈ 0.2 at room temperature [3] to 0.5 at $T > 400$ K [11]. Interestingly, these surface structures have been observed irrespective of the S source. Until now, most of the controversy in this field has been related to the chemical nature of these rectangular-like patterns. These have been successively assigned to reconstructed gold [20], adsorbed S atoms forming S_8-like species [17], gold sulfide [4], a mix of S_2 and monomeric S in a quasi-rectangular arrangement [19], and, more recently, to adsorbed S_2 in different configurations to form S_8-like species [21,22] based on scanning tunneling microscopy (STM), spectroscopic evidence and density functional theory (DFT) calculations. Similar quasi-rectangular polysulfide structures have been observed on the Au(001) surface, and the basic building blocks have been also assigned to S_2 species [23]. However, there are new evidences indicating that the disulfide species are stabilized by gold atoms forming well ordered disulfide-gold complexes [24].

Notably, other S species, such as trimer-like structures, have been observed coexisting with the $(\sqrt{3} \times \sqrt{3})$ R30° S lattice in electrochemical environments [25,26], although their structure and chemistry have not yet been elucidated. In this paper we will focus on the

* Corresponding author at: INIFTA, Argentina.
E-mail addresses: pcarro@ull.edu.es (P. Carro), gandreasen@inifta.unlp.edu.ar (G. Andreasen), cvericat@inifta.unlp.edu.ar (C. Vericat), mevela@inifta.unlp.edu.ar (M.E. Vela), robsalva@inifta.unlp.edu.ar (R.C. Salvarezza).

https://doi.org/10.1016/j.apsusc.2019.05.167
Received 2 August 2018; Received in revised form 8 March 2019; Accepted 15 May 2019
Available online 16 May 2019
0169-4332/

structure and the chemistry of these trimer-like structures, and on how they are related to a new and denser surface structure, as revealed by our combined STM and DFT study.

2. Materials and methods

STM experiments were performed both in air and under electrochemical control (ECSTM) at room temperature by using an ECM microscope and a Nanoscope IIIA controller from Veeco Instruments (Santa Barbara, CA). Imaging was done in the constant current mode with mechanically cut Pt−Ir tips, which were insulated with Apiezon wax. ECSTM imaging was performed by means of a bipotentiostat from Veeco Instruments (Santa Barbara, CA) with a small volume Kel-F cell. A high area Pt wire was used as the counter electrode and a Pd/H_2 electrode as the reference (+0.05 V vs standard hydrogen electrode, SHE). The electrolyte was a deaerated 3×10^{-3} M Na_2S + 0.1 M NaOH solution. Typical setpoint currents and scan rates were 20–30 nA and 10–15 Hz, respectively. Working electrode (E_s) and tip (E_t) potentials were measured with respect to the Pd/H_2 reference, but in the text are referred to the SHE electrode. For in air measurements, typical bias voltages (E_{bias}), setpoint currents and scan rates were 0.05–0.2 V, 5–15 nA and 15–30 Hz, respectively.

Evaporated Au films on glass with (111) preferred orientation (Arrandees™, Germany) were used as substrates. After annealing for 3 min with a hydrogen flame these substrates exhibit atomically smooth (111) terraces separated by monatomic steps in height. The typical terraces width is about 70–100 nm (Fig. S1). However, in some cases there are also smaller terraces, about 20 nm in size. Clean substrates were used as the working electrodes for ECSTM measurements. For in air measurements S layers were formed by immersion of the clean substrates in aqueous 3×10^{-3} M Na_2S + 0.1 M NaOH solution for 10 min at room temperature, which were then rinsed with water and dried with a N_2 flux.

3. Theoretical calculations

Density functional calculations were performed with the periodic plane-wave basis set code VASP 5.2.12 [27,28]. The scheme of non-local functional proposed by Dion et al. [29], vdW-DF, and the optimized Becke88 exchange functional optB88-vdW [30], were used to take into account van der Waals (vdW) interactions. The projector augmented plane wave (PAW) method was used to represent the atomic cores using the PBE potential [31]. The electronic wave functions were expanded in a plane-wave basis set with a 420 eV cutoff energy. Optimal grids of Monkhorst-Pack [32] k-points $7 \times 7 \times 1$ an $1 \times 1 \times 1$ were used for numerical integration in the reciprocal space of the $(\sqrt{7} \times \sqrt{7})$ R19.1° and $(3\sqrt{3} \times 3\sqrt{3})$ R30° unit cells described in the experimental results section. The Au(111)-(1×1) substrate is represented by five ($(\sqrt{7} \times \sqrt{7})$ R19.1°) or four ($(3\sqrt{3} \times 3\sqrt{3})$ R30°) atomic layers and a vacuum of ~17 Å that separates two successive slabs in our calculation. Surface relaxation is allowed in the three uppermost Au layers of the slab, while the atomic coordinates of the adsorbed species were allowed to relax as well without further constraints. The atomic positions were relaxed until the force on the unconstrained atoms was < 0.03 eVÅ^{-1}. Adsorbates were placed just on one side of the slab and all calculations include a dipole correction. The S atom and the AuS_3 complex were optimized in an asymmetric box of 17 Å × 18 Å × 19 Å. The calculated Au lattice constant is 4.16 Å, which compares reasonably well with the experimental value (4.078 Å) [33]. The average binding energy per adsorbed S species on Au(111) surfaces, E_b, is defined in Eq. (1):

$$E_b = \frac{1}{N_S}[E^{S/Au} - E^R_{Au} - N_S E^S] \quad (1)$$

where, $E^{S/Au}$, ${E_{Au}}^R$ and E^S stand for the total energy of the adsorbate-substrate system, the total energy of the Au slab (reconstructed after the S adsorption process), and the energy of the adsorbed S, respectively, whereas N_S is the number of S atoms in the surface unit cell. A negative number indicates that adsorption is exothermic with respect to the separate clean surface and S atom.

The reconstructed energy, $E_{rec,}$ of the surface is defined by,

$$E_{rec} = \frac{E^R_{Au} - E^U_{Au}}{N_S} \quad (2)$$

where ${E_{Au}}^R$, ${E_{Au}}^U$ correspond to the energy of reconstructed Au surface and unreconstructed Au surface per cell unit respectively. Therefore, we define

$$E^*_b = E_b + E_{rec} \quad (3)$$

Moreover, the Gibbs free energy of adsorption of each surface structure (γ) can be approximated through the total energy from DFT calculations and the area (A) by using Eq. (4) [34,35]:

$$\gamma = \frac{N_S}{A} E^*_b \quad (4)$$

Considering that we are concerned with free energy differences, it is reasonable to assume that the contributions arising from the vibrations and the work term *pV,* can be neglected [36,37]. Bader charge analysis of the adsorbed species was also performed by using the algorithm proposed by Henkelman et al. [38].

The simulated STM images of the models were made by using the Tersoff-Hamman method [39] with the STM tip approximated as a point source, under constant current conditions and applying a bias voltage of −40 mV employing the p4vasp software.

4. Results and discussion

Figs. 1a and S1a show STM images taken at E = −0.350 V vs SHE. Domains of a honeycomb-like structure that consists of six bright triangular elements (hexagons) organized around a star-shaped center (dark region in the image) are clearly observed.

The center-to-center distance is ≈1.5 nm, with a maximum height difference between the bright triangular elements and the dark centers of 0.07 nm, i.e. they are not gold atoms and instead can be assigned to adsorbed S species. Similar structures have been reported for S adsorption in electrochemical environments [26]. No evidence of vacancy islands inside the ordered domains is found in the images, as the cross section analysis indicates height differences between dark and bright features that are smaller than 0.24 nm.

High resolution STM images (Fig. 1b) reveal that the triangular elements are formed by three bright spots (trimers) with average nearest neighbor distance d = 0.36 ± 0.03 nm, i.e. a distance too large to be assigned to S−S bonds. Also, in Fig. 1b a small domain of the well-known $(\sqrt{3} \times \sqrt{3})$ R30° lattice formed by monomeric S is shown, which serves as a reference. It is worth to mention that the dark hexagons are rotated 30° in relation to the $(\sqrt{3} \times \sqrt{3})$ R30° lattice, i.e. they follow the substrate direction (see arrows in Fig. 1). Moreover, in some of the trimers one of the spots is brighter than the other two.

We have modeled the honeycomb-like domains as a $(3\sqrt{3} \times 3\sqrt{3})$ R30° lattice, composed of two groups of three S species with a total S coverage θ = 6/27 = 0.22 (green spheres in Fig. 2). This structure is consistent with the experimental orientation of the hexagon motifs, the center-to-center hexagon distances, and also with the S intra-trimer distances.

After geometry optimization of the initial structure we observe that the Au atom located at the center of the 3 S atoms is spontaneously lifted 0.17 nm from the substrate surface, as shown in Fig. 2a-b and S3, thus creating a vacancy in the substrate. The S atoms are placed at nearly bridge sites around the extracted Au atom. Interestingly, the three S atoms interact with the lifted Au atom from the substrate but not among themselves, i.e. they are individual S atoms coordinated by the lifted Au atom. Indeed, the existence of three-coordinated Au

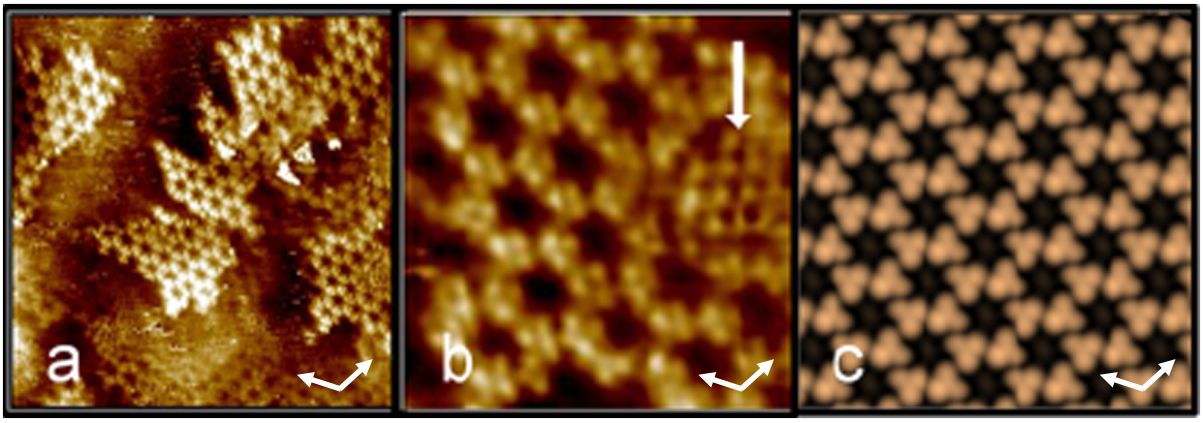

Fig. 1. STM images taken under electrochemical control in 3×10^{-3} M Na_2S + 0.1 M NaOH. E = −0.35 V (SHE). (a) ($28.4 \times 28.4\ nm^2$) honeycomb-like S lattice, (b) ($8 \times 8\ nm^2$). Detail of the trimer structures forming the honeycomb-like lattice. The white arrow indicates a small domain of the ($\sqrt{3} \times \sqrt{3}$)R30° lattice. (c) Simulated STM image of the ($3\sqrt{3} \times 3\sqrt{3}$)R30° lattice model shown in Fig. 2. The small white arrows in the images indicate the orientation of the Au(111) lattice.

complexes has been already reported [40–42]. Also some S atoms in the 3S−Au structures are slightly higher with respect to the Au substrate (Table 1), thus explaining the brighter spots in Fig. 1b.

The energetic and geometric parameters of the proposed model are shown in Table 1. The calculated STM images (Fig. 1c) are in excellent agreement with the experimental data in Fig. 1b. The fact that the Au atom at the central position of the trimers is not "seen" by the STM tip indicates that the density of states at the Fermi level is dominated by the S atom states.

We have also observed a denser S lattice (Fig. 3a-b and S1b) coexisting with the trimers that was also imaged under ambient conditions (Fig. 3c). In this case the S atoms arrange into a quasi-hexagonal pattern (Fig. 3b inset) with average distances d = 0.37 ± 0.03 nm, i.e. the same distances as in the trimers of the honeycomb-like S structure. Also in this case we did not observe vacancy islands in the ordered domains. Indeed, the cross section analysis along the black regions in Fig. 3a yields height differences ≈0.1 nm, smaller than the depth expected for gold vacancy islands (0.24 nm), and which can instead be assigned to missing S atoms. An interesting observation in Fig. 3a, b and S1b is the presence of some dark centers arranged with distances consistent with the ($3\sqrt{3} \times 3\sqrt{3}$) R30° lattice proposed for the less dense S overlayer shown in Fig. 1. In this sense, the images in Fig. 3a and b show the transition from the diluted to the denser surface structures.

We have modeled this surface structure with a ($\sqrt{7} \times \sqrt{7}$) R19° lattice with a sulfur coverage θ = 4/7 = 0.57 which yields S−S distances similar to the experimental ones. Note that a diffuse phase has been observed by LEED at this surface coverage [43]. Interestingly, here also the initial hexagonal lattice is spontaneously distorted as a result of the optimization procedure. Indeed, one Au atom is lifted 0.24 nm from the substrate surface to form 3S−Au species similar to those described for the ($3\sqrt{3} \times 3\sqrt{3}$) R30° lattice (Fig. 4). Two S atoms of the 3S−Au structures are located at nearly bridge sites, while the remaining one is placed at an on-top site. The lattice is completed with one S atom adsorbed at fcc-hollow site. The energetic and geometric parameters of the ($\sqrt{7} \times \sqrt{7}$)R19° lattice model are summarized in Table 1. Again, the simulated STM image is in excellent agreement with those observed in the experiments (Fig. 3d). However, there is a subtle difference between the STM simulation of the ($3\sqrt{3} \times 3\sqrt{3}$) R30° lattice (Fig. 1c) and that shown in Fig. 3d. Despite the fact that the both simulations were made under the same conditions, the Au adatom is appreciable in the simulation of the ($\sqrt{7} \times \sqrt{7}$) R19° as a small spot (red spot in Fig. 3d) while it is not present in the simulation of the ($3\sqrt{3} \times 3\sqrt{3}$) R30° lattice (Fig. 1c). The origin of this difference can be found in the greater S coverage of this surface structure, that gives rise to small differences in the Bader charge of the respective Au adatoms (Table S1), and also in slight structural differences (Table S2). In fact, the position of the Au

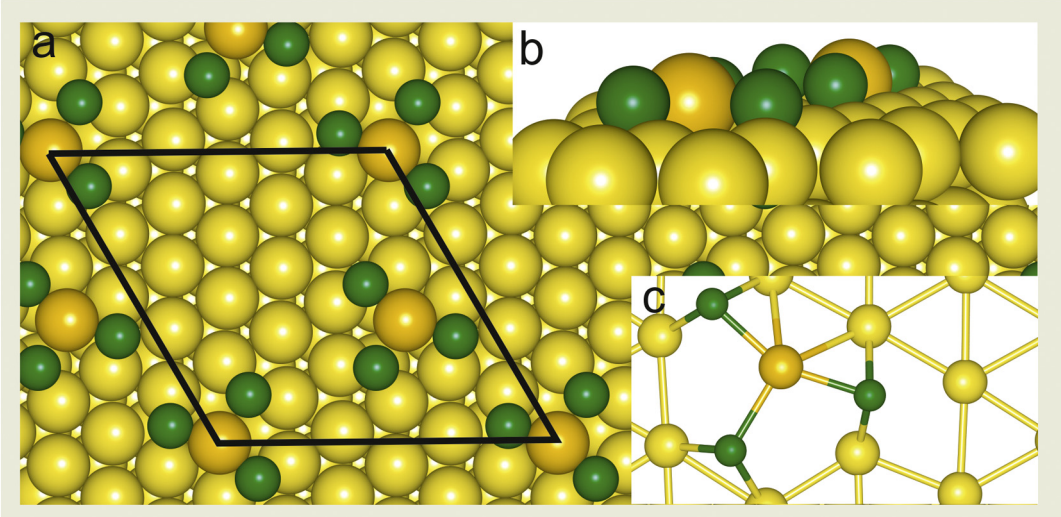

Fig. 2. Optimized structures of the ($3\sqrt{3} \times 3\sqrt{3}$) R30° honeycomb lattice. (a) top view, (b) side view (c) detail of the optimized geometry. Yellow: Au atoms, orange: lifted Au atom, green: S atoms. The unit cell is indicated (solid black lines).

Table 1
Energetic and geometric parameters of the different surface species and gold complexes.

Model	S/Au(111)				S_3Au (gas)
Surface lattice	(3√3 × 3√3) R30°		(√3 × √3) R30°	(√7 × √7) R19.1°	(17 × 18 × 19)
θ_S	0.22	0.33	0.33	0.57	–
E_b/eV	−4.19	−4.14	−3.63	−3.81	−2.51
E_{rec}/eV	+0.60	+0.56	0.0	+0.48	–
γ/meV·Å^{-2}	−106.6	−159.61	−161.71	−254.0	–
d(S–S)/Å	3.8[a]	3.8[a]	5.0	3.6/4.2	3.8
d(Au_{ad}-S)/Å	2.4/2.4/2.5	2.4/2.4/2.5	–	2.4/2.4/2.3	2.2
Δz(S-surface)/Å	1.8/1.7/1.8 1.9/1.8/1.8	1.8/1.9/1.7 1.8/1.8/1.7 1.8/1.8/1.7	1.6	2.3/1.9/2.0 1.5 (hollow (111)	–
α(S-Au-S)°	155/103/103	154/102/102	–	159/100/100	120

[a] Intra trimer S distance, nearest neighbor S distance inter trimers 4.6 Å.

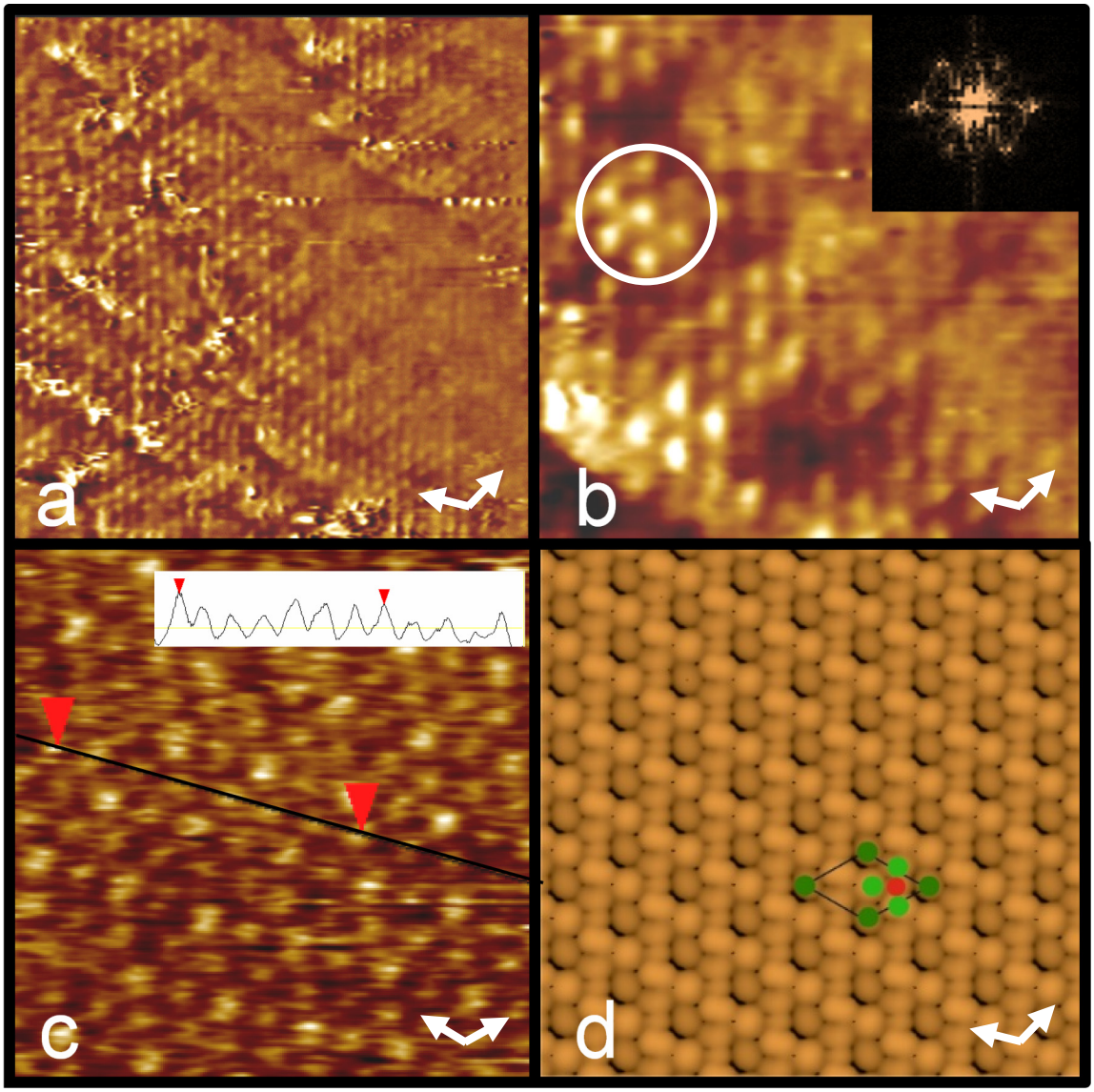

Fig. 3. In situ STM images taken at E = −0.350 V (vs SHE) in 3×10^{-3} M Na_2S + 0.1 M NaOH (a) (12.2 × 12.2 nm^2) showing the dense hexagonal S lattice, (b) (4.6 × 4.6 nm^2). The S atom arrangement is depicted in more detail. Inset: Fourier transform analysis showing the hexagonal pattern, (c) STM image taken in ambient conditions (4.6 × 4.6 nm^2), inset: cross section showing the 0.37 nm periodicity (the distance between the red arrows is 2.5 nm), (d) simulated STM image of the (√7 × √7)R19° lattice model shown in Fig. 4. The small white arrows in the images indicate the orientation of the Au(111) lattice. The unit cell is indicated. Light green: S atom in the 3S–Au species, red: Au adatom, green: monomeric S atoms.

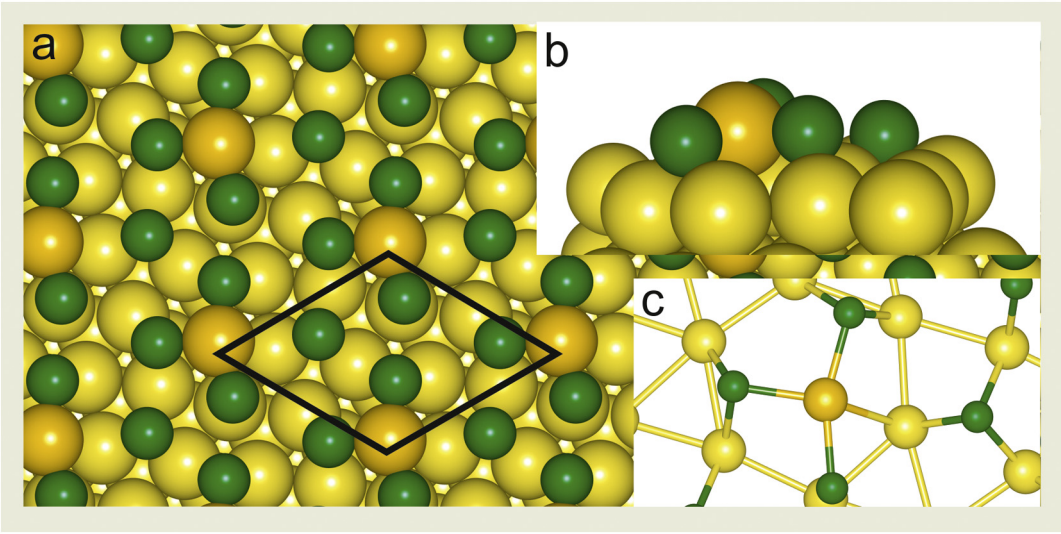

Fig. 4. Optimized structure of the (√7 × √7)R19° lattice model. (a) top view, (b) side view (c) detail of the optimized geometry. Yellow: Au atoms, orange: lifted Au atom, green: S atoms. The unit cell is indicated (solid black lines).

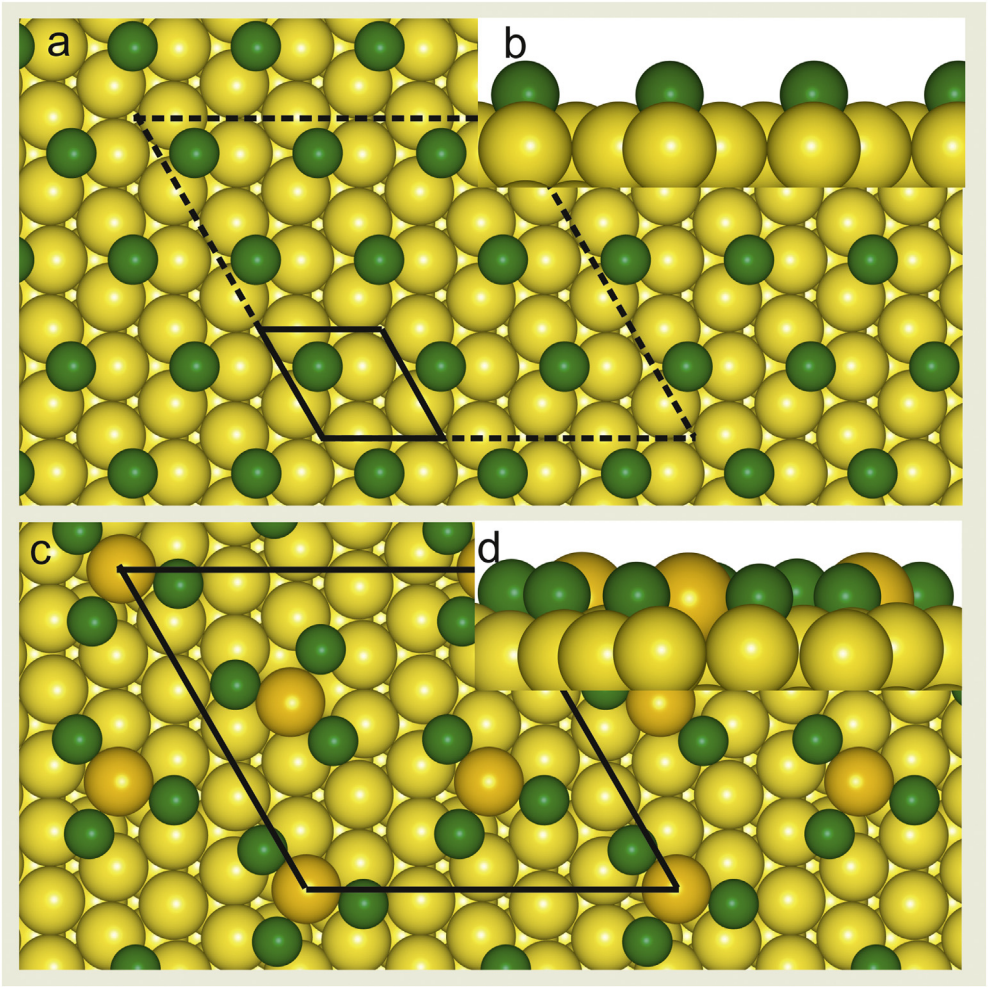

Fig. 5. Optimized structure of the (√3 × √3) R30° surface lattice. (a) top view, (b) side view. Complete (3√3 × 3√3) R30° lattice (c) top view, (d) side view. Yellow: Au atoms, orange: lifted Au atom, green: S atoms. The unit cells are indicated (solid black lines). In Fig. 5a the solid line represents the real lattice and the dashed line the one used in the DFT calculations.

adatom with respect to both S and Au substrate atoms is higher in the (√7 × √7) R19° than in the (3√3 × 3√3) R30° lattice (Table S2). Also in this case some S atoms have different height relative to the substrate, explaining the different contrast in the STM images (Table 1).

For coverage θ = 0.33, S atoms are adsorbed at fcc-hollow site, forming the well-known (√3 × √3) R30° lattice. In order to compare the results of the present work with those on an unreconstructed Au (111) surface performed under the same calculation conditions (lattice, metal layer number, k points, vacuum layer) we have calculated the energetic and geometric parameters of a (3√3 × 3√3) R30°-S lattice with the S atoms located at fcc-hollow site and S coverage, θ = 0.33, i.e. corresponding to the (√3 × √3) R30° lattice (see Table 1 and Fig. 5a and b). Our DFT calculations show that, although the (3√3 × 3√3) R30° 3S−Au honeycomb lattice with θ = 0.22 exhibits a higher E_b than that corresponding to the (√3 × √3) R30° lattice, there is an energetic cost, E_{rec}, derived from the lifting of the Au adatom from the topmost layer of the surface. This, together with the fact that its coverage is lower, accounts for a more positive γ value (see Eqs. (1)–(4) of the (3√3 × 3√3)R30° honeycomb lattice compared to the (√3 × √3)R30° lattice, i.e. the former is thermodynamically less stable. On the other hand, the (√7 × √7) R19° surface structure has a similar E_b value as that shown by the (√3 × √3) R30° and exhibits a considerable E_{rec} value. However, this structure compensates the high cost to reconstruct its surface with its higher S coverage, θ = 0.57, which leads it to present the highest stability in terms of surface free energy among the structures studied in this work.

In this context it is important to discuss why the 3S−Au islands can coexist with the (√3 × √3)R30°- S lattice, which is more stable in terms of the energetic parameters here considered (Fig. 1b). First, we note that there are several equivalent configurations for S positions in the 3S−Au structures forming the (3√3 × 3√3)R30° honeycomb lattice which are compatible with the experimental STM images. We have estimated the stability of another surface structure in which the orientation of the two triangles in the unit cell is the same and have found that this is only 4 meV A^{-2} more unstable than that determined for the model proposed in Fig. 4, i.e. the system only changes slightly in terms of energetic parameters.

It has been shown that the configurational entropy restricts the validity of an analysis based only on energetic considerations for temperatures above 0 K [44]. This term of the free energy calculation is difficult to estimate [45], but could qualitatively explain why relatively dense islands of adsorbates prevail over more extended diluted domains [44,46]. In principle, this argumentation cannot be applied in this case, as our experimentally observed (3√3 × 3√3)R30° honeycomb lattice is more diluted (θ = 0.22) than the (√3 × √3)R30° lattice (θ = 0.33). However, Stickney et al. have observed a complete (3√3 × 3√3)R30° lattice with θ = 0.33 [26], which can be also modeled with 3S−Au species. We have calculated this complete (3√3 × 3√3)R30°-3S-Au lattice (Fig. 5c–d) and after optimization obtained $E_b = -4.14$ eV and $\gamma = -159.6$ meV $Å^{-2}$, i.e. the lattice is similar in stability to the (√3 × √3)R30°-S lattice on the unreconstructed Au(111) ($\gamma = -161.7$ meV $Å^{-2}$). Even if the complete (3√3 × 3√3)R30° is slightly less stable than the (√3 × √3)R30° lattice, the contribution of its configurational entropy can account for the coexistence of (3√3 × 3√3)R30°-3S-Au and (√3 × √3)R30°-S domains. A slow adsorption kinetics could be the reason why we observe the (3√3 × 3√3) R30° honeycomb lattice (θ = 0.22) in our in situ STM images rather than the complete (3√3 × 3√3)R30° structure (θ = 0.33) imaged by Stickney et al.

In order to compare the stability of the surface structures studied in this work with the well-known octomeric structures in a (3 × 2√3) lattice with surface coverage 0.66, we have made an estimation of their thermodynamic stability. This lattice is actually formed by S_2 and monomeric S species and has an Au atom lifted from the substrate as well [19]. Thus, by using Eq. (4) and the E_b value reported in that work it results in $\gamma \approx -300$ meV $Å^{-2}$, i.e. the (3 × 2√3) surface structure is more stable than the (√7 × √7) R19° S lattice. Although, the comparison of this γ value with those reported in the present work should be taken with care due to the different computational methodologies, it seems to be a reasonable comparison as the E_b value for the (√3 × √3)R 30° is similar in both cases.

Finally, it is important to stress that the 3S−Au species considered in this work are not a two-dimensional gold sulfide phase, which was one of the models proposed for 8 S on Au(111) at high sulfur coverage [4,47]. Also, they cannot be identified with the Au_3S_3 clusters observed for the initial S adsorption of S at liquid nitrogen temperature [48].

We have made a charge analysis of the honeycomb (3√3 × 3√3) R30° and (√7 × √7) R19° lattices (Table S1). In the former case the Bader charge analysis indicates a charge transfer from the lifted Au atom to the S atoms in the 3S−Au structures. In fact, a charge of −0.27/−0.30 e is obtained for the S atoms and +0.26/+0.27 e for the central Au atom. Note that the Au atoms in the top layer have a considerably lower charge (+0.05 e). As regards the (√7 × √7) R19° lattice, given its smaller size and greater S coverage, it has all the top layer Au atoms involved in the bonding, either with one or two S atoms or with the lifted Au atom, a situation that results in a greater complexity

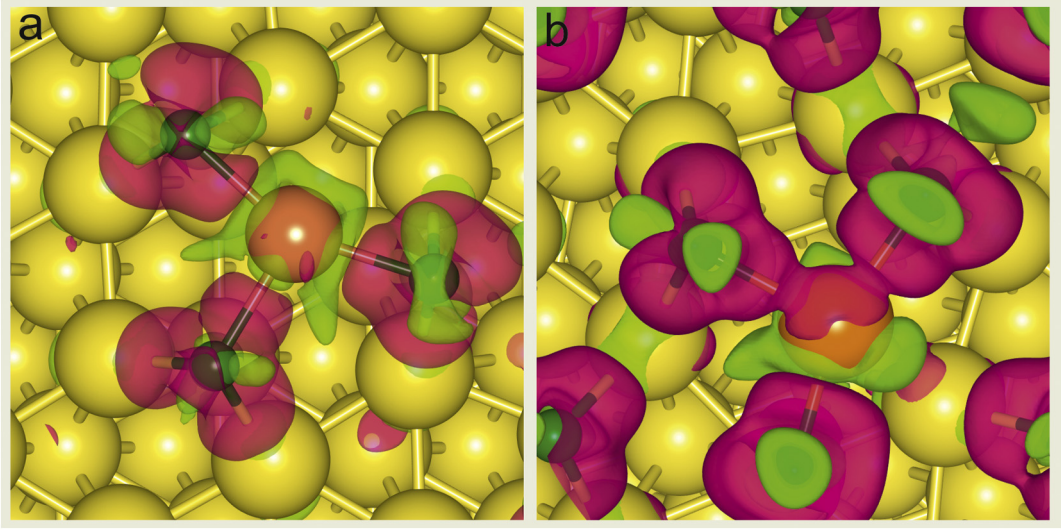

Fig. 6. Charge density difference isosurfaces for the a) S- (3√3 × 3√3) R30° lattice and b) S-(√7 × √7) R19 ° lattices on Au(111) showing electronic charge accumulation (pink) and depletion (green).

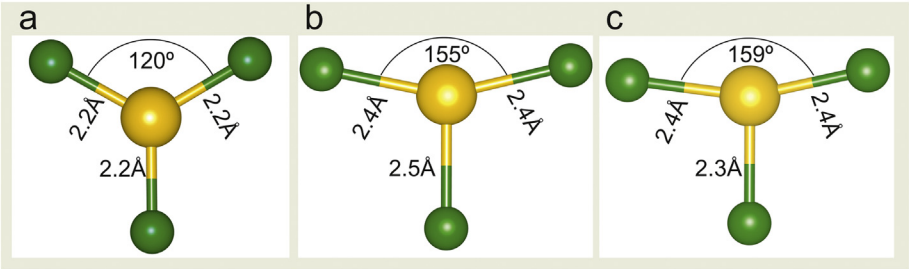

Fig. 7. (a) AuS_3 complex. 3S−Au structures as found (o formed) in the (b) (3√3 × 3√3) R30° and (c) (√7 × √7) R19° lattices. Orange: Au atom, green: S atoms.

in the distribution of the surface atom charge. Thus, the charge of S atoms bonded to the lifted Au atom are −0.28 e and −0.22/−0.24 e at on-top and bridge sites, respectively, very similar to the Bader charge of the isolated S atom placed in a hollow fcc site of the surface (−0.21). In addition, the Bader charge results in +0.33 e for the lifted Au atom, while it changes between +0.17 e and +0.07 e for the other Au surface. These data should be compared to those corresponding to the (√3 × √3) R30° lattice on the unreconstructed surface, where the S atom at fcc-hollow has −0.29 e and the subjacent Au substrate atoms exhibit +0.10 e.

The charge density difference isosurfaces of the adsorbed species show more clearly the S charge density accumulation for both models (Fig. 6a–b). From these data one can conclude that the charge of the adsorbed S atoms remains nearly unchanged (≈ −0.28 e/−0.22 e) in the different surface structures. In contrast, there are marked differences in the charge of the Au atoms: while the metal substrate atoms have +0.07/+0.17, irrespective of the lattice, the Au lifted atoms exhibit much larger charges: +0.26 e in the honey-like lattice and +0.33 e in the (√7 × √7) R19° lattice. This ≈behavior reveals the distinctive character of the Au adatom lifted from the surface compared with the Au atoms the substrate.

Following this line of reasoning, we have also studied the electronic structure of 3S−Au species in the gas phase in order to analyze its stability as an isolated AuS_3 complex (Fig. 7), i.e., in the absence of the Au substrate (Table 1). It is well-known that trigonal-planar-coordinated Au(I) centers have interesting photoemission properties and also important applications as antiarthritic and cancerostatic drugs [49]. We have found that this complex is stable and that it adopts a C3v symmetry with S−Au distances of 0.22 nm and an angle α(S-Au-S) = 120° (Fig. 7a Table 1). The S−Au bond energy is −2.51 eV, and the S−Au distances are slightly smaller than those in the similar trigonal 3S−Au structures adsorbed on the Au(111) surface (Fig. 7b–c, Table 1). Likewise, bond angles (S-Au-S) are distorted in the presence of the surface in order to achieve the most favorable configuration (Table 1). These facts seem to indicate the relevant influence of the substrate and its competition for S atoms of the complex. Interestingly, the Bader charges of the isolated complex are very similar to those on the Au(111) surface. In fact, they are +0.42 e and −0.17 e for the Au and S atoms, respectively. This means that most of the charge transfer of the adsorbed species takes place between the S atoms and the Au adatom. Therefore, we propose that the 3S−Au species can be considered as AuS_3 complexes distorted by the substrate interaction.

In order to better understand the role of the substrate reconstruction on the 3S−Au stability, we have calculated the energetics of the adsorption of two 3S−Au species on (3√3 × 3√3) R30° lattice on a unreconstructed Au(111). In this configuration there would be no need to extract the Au atom from the Au(111) surface to form the 3S−Au complex. However, in this case the 3S−Au structures result unstable and evolve towards S-Au-S complexes and adsorbed S atoms. S−S distances are larger than those experimentally observed and there is no significant gain in surface free energy. This is a clear evidence that the surface reconstruction and the structural vacancy actually stabilize the 3S−Au structures. Note that a recent theoretical work predicts that S-Au-S complexes cannot be formed, as adsorbed atomic S is more stable on the Au(111) surface [50]. Our results show that S_3Au complexes co-adsorbed with atomic S can form well-ordered lattices with a high thermodynamic stability, even though they require surface reconstruction and structural vacancies to stabilize the system.

Now we can discuss the origin of the Au vacancy islands. It has been proposed that the 8S structures formed by adsorbed S_2 and monomeric S species with surface coverage θ = 0.66 are able to lift one gold atom from the substrate every 8 S atoms [19]. Although, this is in qualitative agreement with the lifting of Au atoms proposed here, it is not possible to explain the final coverage of gold vacancy islands observed in the STM images ($\theta_{vac} \approx 0.2$; see Fig. S2) based on their structure, as they only provide a vacancy coverage $\theta_{vac} = 0.08$, which is too far from the experimental value. On the other hand, the (√7 × √7) R19° lattice has $\theta_{ad} = 1/7 = 0.14$, i.e., there is one adatom for every 4 S species (S_3 + S), and one structural vacancy associated. We therefore propose that AuS_3 complexes are intermediate species in going from the (√7 × √7) R19° lattice to the denser and thermodynamically more stable 8S polysulfide surface structures [19]. This transformation leaves the single vacancies that are now free to diffuse and to nucleate as vacancy islands (at terraces) or to be adsorbed at step edges in order to decrease the surface free energy. As above mentioned the (√7 × √7) R19° provides an amount of single vacancies equivalent to $\theta_{vac} = 0.14$, much closer to the experimental data. The islands grow by adsorbing more vacancies or by coalescence, as observed by in situ STM images at S-containing organic molecules adsorbed on Au(111) terraces.

On this basis, we can conclude that the well-known (√3 × √3) R30° S lattice coexists with the (3√3 × 3√3) R30° lattice formed by AuS_3 complexes. This intermediate surface structure is stabilized by incorporating more S atoms to yield the denser (√7 × √7) R19° lattice, which contains both AuS_3 structures and monomeric S, as schematically shown in Fig. 8. This process involves translation and rotation of the AuS_3 complexes.

The stability of the AuS_3 complexes not only arises out of the charge transfer from the lifted Au atom to the S atoms but also because of their interaction with the reconstructed substrate surface where the structural vacancy plays an stabilizing role. The addition of more S atoms to

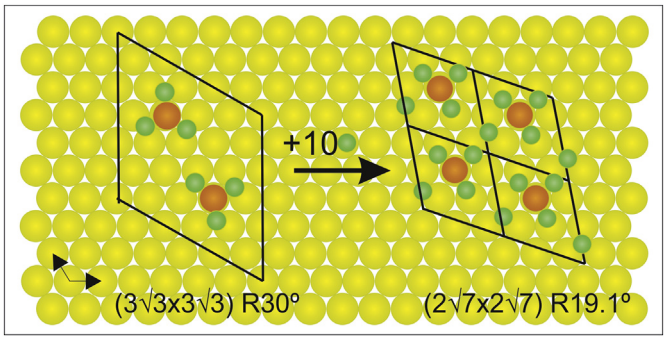

Fig. 8. Scheme showing the relationship between the AuS_3 containing lattices on Au(111). Yellow: Au atoms, orange: lifted Au atom, green: S atoms.

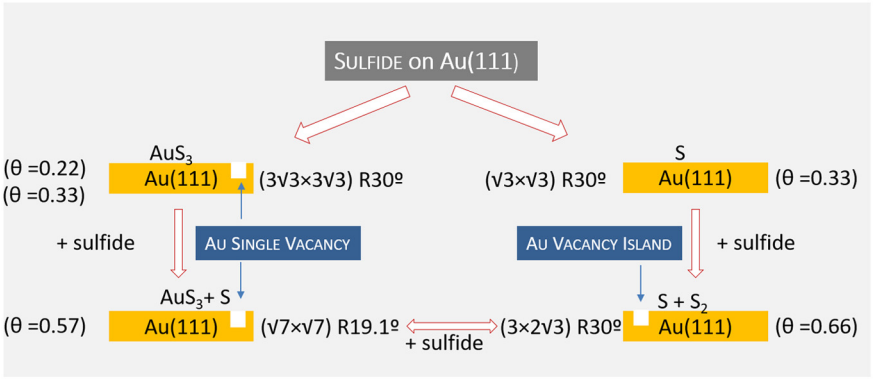

Fig. 9. Scheme showing the relationship among the different S surface structures on Au(111) that were observed by STM. Au vacancy islands are included for structures that induce surface reconstruction.

the (√7 × √7) R19° lattice would certainly result in the formation of disulfide species (S—S distances 0.2 nm). Therefore, the system reorganizes into the well-known and more stable 8S rectangular structures containing S_2, S and some Au atoms, leaving the single vacancies free to diffuse and to form the vacancy islands. This interpretation explains the coverage of vacancy islands experimentally observed on Au (111) surface, which cannot be solely understood on the basis of the 8S structures.

These conclusions from our work can be summarized by the reaction scheme in Fig. 9, which accounts for all features, S lattices and Au vacancies, with their corresponding coverage, observed in the STM images.

These results, and those recently reported by our group [24], allow a deeper understanding of the sulfur-gold chemistry in 2D systems. Indeed, adsorbates include monomeric sulfur, monomeric sulfur-gold complexes, adsorbed disulfides and disulfide-gold complexes, and the substrate plays a significant role in the adsorbate geometry. It could be argued that the solvent, electrolyte, and electric field could have a key in the formation of surface structures. However, we have imaged the (√7 × √7)R19° lattice both in electrolyte and air environments, as shown in Fig. 3. Moreover, the (4 × 4) lattice, similar to our (3√3 × 3√3)R30° lattice, has been observed by LEED on Au(111) exposed to SO_2 [43]. In any case, we cannot exclude that the cations from the electrolyte and the applied potential play a role, as discussed in Ref [26].

5. Conclusions

We have presented a combined STM and DFT study that reveals the existence of two new surface structures formed by gold-sulfur complexes, which can coexist with adsorbed S atoms. We believe that these results contribute to provide a unified picture of the S—Au interface in S-containing adsorbates, thus helping to find a bridge from the surface chemistry of sulfur to that of sulfur-containing molecules, such as thiols on Au(111), for which the existence of gold-thiolate complexes [51] and adsorbed radicals is still a matter of controversy [52,53].

Acknowledgments

Authors acknowledge financial support from ANPCyT (PICT 2016-0679) Argentina, CONICET (PIP 0093) Argentina, Universidad Nacional de La Plata (11X760) Argentina and MINECO (ENE2016-74889-C4-2-R, AEI-FEDER-UE) Spain. MEV is member of the research career of CICPBA. PC thankfully acknowledges the computer resources provided by the Computer Support Service for Research (SAII) at La Laguna University.

Appendix A. Supplementary data

Supplementary data to this article can be found online at https://doi.org/10.1016/j.apsusc.2019.05.167.

References

[1] J.A. Rodriguez, J. Hrbek, Interaction of sulfur with well-defined metal and oxide surfaces: unraveling the mysteries behind catalyst poisoning and desulfurization, Acc. Chem. Res. 32 (1999) 719–728.
[2] J.A. Rodriguez, J. Dvorak, T. Jirsak, G. Liu, J. Hrbek, Y. Aray, C. González, Coverage effects and the nature of the metal−sulfur bond in S/Au(111): high-resolution photoemission and density-functional studies, J. Am. Chem. Soc. 125 (2003) 276–285.
[3] E. Pensa, E. Cortés, G. Corthey, P. Carro, C. Vericat, M.H. Fonticelli, G. Benítez, A.A. Rubert, R.C. Salvarezza, The chemistry of the sulfur-gold interface: in search of a unified model, Acc. Chem. Res. 45 (2012) 1183–1192.
[4] M.M. Biener, J. Biener, C.M. Friend, Revisiting the S-Au(111) interaction: static or dynamic? Langmuir 21 (2005) 1668–1671.
[5] H. Walen, D.-J. Liu, J. Oh, H. Lim, J.W. Evans, Y. Kim, P.A. Thiel, Self-organization of S adatoms on Au(111): √3R30° rows at low coverage, J.Chem.Phys. 143 (2015) 014704.
[6] M. Yu, H. Ascolani, G. Zampieri, D.P. Woodruff, C.J. Satterley, R.G. Jones, V.R. Dhanak, The structure of atomic sulfur phases on Au(111), J.Phys.Chem C 111 (2007) 10904–10914.
[7] K.M. Koczkur, E.M. Hamed, A. Houmam, Sulfur multilayer formation on Au(111): new insights from the study of hexamethyldisilathiane, Langmuir 27 (2011) 12270–12274.
[8] J.E. Bailie, G.J. Hutchings, Promotion by sulfur of gold catalysts for crotyl alcohol formation from crotonaldehyde hydrogenation, Chem. Commun. (1999) 2151–2152.
[9] S. Schimpf, M. Lucas, C. Mohr, U. Rodemerck, A. Brückner, J. Radnik, H. Hofmeister, P. Claus, Supported gold nanoparticles: in-depth catalyst characterization and application in hydrogenation and oxidation reactions, Catal. Today 72 (2002) 63–78.
[10] R. Meyer, C. Lemire, S.K. Shaikhutdinov, H.-J. Freund, Surface chemistry of catalysis by gold, Gold Bull. 37 (2004) 72–124.
[11] B.K. Min, A.R. Alemozafar, M.M. Biener, C.M. Biener, C.M. Friend, Reaction of Au (111) with sulfur and oxygen: scanning tunneling microscopic study, Top. Catal. 36 (2005) 77–90.
[12] M.A. Huergo, L. Giovanetti, M.S. Moreno, C.M. Maier, F.G. Requejo, R.C. Salvarezza, C. Vericat, New insight into the chemical nature of the plasmonic nanostructures synthesized by the reduction of Au(III) with sulfide species, Langmuir 33 (2017) 6785–6793.
[13] M.A. Huergo, C.M. Maier, M.F. Castez, C. Vericat, S. Nedev, R.C. Salvarezza, A.S. Urban, J. Feldmann, Optical nanoparticle sorting elucidates synthesis of plasmonic nanotriangles, ACS Nano 10 (2016) 3614–3621.
[14] B. Pelaz, V. Grazu, A. Ibarra, C. Magen, P. del Pino, J.M. de la Fuente, Tailoring the synthesis and heating ability of gold nanoprisms for bioapplications, Langmuir 28 (2012) 8965–8970.
[15] P.A. Thiel, M. Shen, D.-J. Liu, J.W. Evans, Adsorbate-enhanced transport of metals on metal surfaces: oxygen and sulfur on coinage metals, J. Vac. Sci. Technol. A 28 (2010) 1285–1298.
[16] G.M. McGuirk, H. Shin, M. Caragiu, S. Ash, P.K. Bandyopadhyay, R.H. Prince, R.D. Diehl, Au(111) surface structures induced by adsorption: LEED I(E) analysis of (1×1) and (5×5) Au(111)–S phases, Surf. Sci. 610 (2013) 42–47.
[17] C. Vericat, G. Andreasen, M.E. Vela, R.C. Salvarezza, Dynamics of potential-dependent transformations in sulfur adlayers on Au(111) electrodes, J.Phys.Chem.B 104 (2000) 302–307.
[18] X. Gao, Y. Zhang, M.J. Weaver, Observing surface chemical transformations by atomic-resolution scanning tunneling microscopy: sulfide electrooxidation on Au

(111), J. Phys. Chem. 96 (1992) 4156–4159.
[19] P.G. Lustemberg, C. Vericat, G.A. Benitez, M.E. Vela, N. Tognalli, A. Fainstein, M.L. Martiarena, R.C. Salvarezza, Spontaneously formed sulfur adlayers on gold in electrolyte solutions: adsorbed sulfur or gold sulfide? J.Phys.Chem C 112 (2008) 11394–11402.
[20] R.L. McCarley, Y.T. Kim, A.J. Bard, Scanning tunneling microscopy and quartz crystal microbalance studies of gold exposed to sulfide, thiocyanate, and n-octadecanethiol, J.Phys.Chem. 97 (1993) 211–215.
[21] C.E. Hernandez-Tamargo, A.L. Montero-Alejo, D.C. Pujals, H. Mikosch, M.P. Hernández, Sulfur dimers adsorbed on Au(111) as building blocks for sulfur octomers formation: a density functional study, J.Chem.Phys. 141 (2014) 044713.
[22] C.E. Hernandez-Tamargo, R. Barzaga, H. Mikosch, J.A. Martínez, J.A. Herrera, M.H. Farías, M.P. Hernández, Density functional theory simulation of the adsorption of sulphur multilayers on Au(100), PCCP 18 (2016) 29987–29998.
[23] J.A. Martínez, J. Valenzuela B, R. Cao Milán, J. Herrera, M.H. Farías, M.P. Hernández, A scanning tunneling microscopy investigation of the phases formed by the sulfur adsorption on Au(100) from an alkaline solution of 1,4-piperazine(bis)-dithiocarbamate of potassium, Appl. Surf. Sci. 320 (2014) 287–293.
[24] F. Lobo Maza, P. Carro, C. Vericat, K. Kern, R.C. Salvarezza, D. Grumelli, Role of gold adatoms in the adsorption of sulfide species on the gold(001)-hex surface, J.Phys.Chem C 122 (2018) 2207–2214.
[25] C. Vericat, M.E. Vela, G.A. Andreasen, R.C. Salvarezza, F. Borgatti, R. Felici, T.L. Lee, F. Renner, J. Zegenhagen, J.A. Martin-Gago, Following adsorption kinetics at electrolyte/metal interfaces through crystal truncation scattering: sulfur on Au (111), Phys. Rev. Lett. 90 (2003) 075506.
[26] M.D. Lay, K. Varazo, J.L. Stickney, Formation of sulfur atomic layers on gold from aqueous solutions of sulfide and thiosulfate:studies using EC-STM, UHV-EC, and TLEC, Langmuir 19 (2003) 8416–8427.
[27] G. Kresse, J. Hafner, Ab initio molecular dynamics for open-shell transition metals, Phys.Rev.B 48 (1993) 13115–13118.
[28] G. Kresse, J. Furthmüller, Efficiency of ab-initio total energy calculations for metals and semiconductors using a plane-wave basis set, Comput.Mat.Sci. 6 (1996) 15–50.
[29] M. Dion, H. Rydberg, E. Schröder, D.C. Langreth, B.I. Lundqvist, Van der Waals density functional for general geometries, Phys. Rev. Lett. 92 (2004) 246401.
[30] J. Klimeš, D.R. Bowler, A. Michaelides, A critical assessment of theoretical methods for finding reaction pathways and transition states of surface processes, J. Phys. Condens. Matter 22 (2010) 074203.
[31] P.E. Blöchl, Projector augmented-wave method, Phys.Rev.B 50 (1994) 17953–17979.
[32] H.J. Monkhorst, J.D. Pack, Special points for Brillouin-zone integrations, Phys.Rev.B 13 (1976) 5188–5192.
[33] W.B. Pearson, Handbook of Lattice Spacing and Structure of Metals, Pergamon Press, Inc, New York, 1958.
[34] D. Torres, P. Carro, R.C. Salvarezza, F. Illas, Evidence for the formation of different energetically similar atomic structures in Ag(111)-(V7xV7)-R19.1°-CH3S, Phys. Rev. Lett. 97 (2006) 226103.
[35] P. Carro, D. Torres, R. Diaz, R.C. Salvarezza, F. Illas, Mechanisms of defect generation and clustering in CH_3S self-assembled monolayers on Au(111), J.Phys.Chem.Lett. 3 (2012) 2159–2163.
[36] H. Aitchison, H. Lu, S.W.L. Hogan, H. Früchtl, I. Cebula, M. Zharnikov, M. Buck, Self-assembled monolayers of oligophenylenecarboxylic acids on silver formed at the liquid–solid Interface, Langmuir 32 (2016) 9397–9409.
[37] A. Shaporenko, A. Terfort, M. Grunze, M. Zharnikov, A detailed analysis of the photoemission spectra of basic thioaromatic monolayers on noble metal substrates, J. Electron Spectrosc. Relat. Phenom. 151 (2006) 45–51.
[38] G. Henkelman, A. Arnaldsson, H. Jónsson, A fast and robust algorithm for Bader decomposition of charge density, Comput.Mat.Sci. 36 (2006) 354–360.
[39] J. Tersoff, D.R. Hamann, Theory of the scanning tunneling microscope, Phys.Rev.B 31 (1985) 805–813.
[40] G. Agbeworvi, Z. Assefa, R.E. Sykora, J. Taylor, C. Crawford, Higher coordinate gold(I) complexes with the weak Lewis base tri(4-fluorophenyl) phosphine. Synthesis, structural, luminescence, and DFT studies, J. Mol. Struct. 1108 (2016) 508–515.
[41] O. Crespo, M.C. Gimeno, A. Laguna, P.G. Jones, Two-, three- and four-co-ordinate gold(I) complexes of 1,2-bis(diphenylphosphino)-1,2-dicarba-closo-dodecaborane, J. Chem. Soc. Dalton Trans. (10) (1992) 1601–1605.
[42] M. Viotte, B. Gautheron, M.M. Kubicki, Y. Mugnier, R.V. Parish, New iron(II)- and gold(I)-containing metallocenes. X-ray structure of a three-coordinate gold(I) ferrocenophane-type representative, Inorg. Chem. 34 (1995) 3465–3473.
[43] G.M. McGuirk, PhD Thesis, in, The Pennsylvania State University, 2011.
[44] P.N. Abufager, G. Zampieri, K. Reuter, M.L. Martiarena, H.F. Busnengo, Long-range periodicity of S/Au(111) structures at low and intermediate coverages, J.Phys.Chem C 118 (2014) 290–297.
[45] K. Reuter, C. Stampfl, M. Scheffler, Ab initio thermodynamics and statistical mechanics of surface properties and functions, in: S. Yip (Ed.), Handbook of Materials Modeling, Part a. Methods, Springer, Berlin, 2005.
[46] A.P.J. Jansen, Island formation without attractive interactions, Phys.Rev.B 77 (2008) 073408.
[47] S.Y. Quek, M.M. Biener, J. Biener, J. Bhattacharjee, C.M. Friend, U.V. Waghmare, E. Kaxiras, Rich coordination chemistry of Au adatoms in gold sulfide monolayer on Au(111), J.Phys.Chem.B 110 (2006) 15663–15665.
[48] S. Kurokawa, Y. Miyawaki, A. Sakai, Scanning tunneling microscopy observation of sulfur adsorbates on Au(111) at liquid nitrogen temperature, Jpn. J. Appl. Phys. 48 (2009) 08JB12.
[49] K. Köhler, S.J. Silverio, I. Hyla-Kryspin, R. Gleiter, L. Zsolnai, A. Driess, G. Huttner, H. Lang, Trigonal-planar-coordinated organogold(I) complexes stabilized by organometallic 1,4-diynes:reaction behavior, structure, and bonding, Organometallics 16 (1997) 4970–4979.
[50] J. Lee, J.S. Boschen, T.L. Windus, P.A. Thiel, D.-J. Liu, Stabilization of X–Au–X complexes on the Au(111) surface: a theoretical investigation and comparison of X = S, Cl, CH_3S, and SiH_3S, J.Phys.Chem C 121 (2017) 3870–3879.
[51] H. Häkkinen, The gold-sulfur interface at the nanoscale, Nat.Chem. 4 (2012) 443–455.
[52] J.R. Reimers, M.J. Ford, A. Halder, J. Ulstrup, N.S. Hush, Gold surfaces and nanoparticles are protected by Au(0)-thiyl species and are destroyed when Au(I)-thiolates form, Proc. Natl. Acad. Sci. U. S. A. 113 (2016) E1424–E1433.
[53] P. Carro, X. Torrelles, R.C. Salvarezza, A novel model for the ($\sqrt{3}\times\sqrt{3}$) R30 alkanethiolate-Au(111) phase based on alkanethiolate-Au adatom complexes, PCCP 16 (2014) 19017–19023.